X CONGRESSO NACIONAL DE ENGENHARIA MECÂNICA 2018
ABCM
20 A 24 DE MAIO DE 2018 SALVADOR – BA – BRASIL

AERODYNAMIC HEATING OF SARA SUB-ORBITAL PLATFORM CONSIDERING CHEMICAL EQUILIBRIUM

Humberto Araujo Machado[1,2]
[1]Instituto de Aeronáutica e Espaço – IAE, São José dos Campos, SP, Brazil
[2]Universidade do Estado do Rio de Janeiro – UERJ, Faculdade de Tecnologia – FAT, Resende, RJ, Brazil
humbertoham@fab.mil.br

Abstract. *In this work, the aerodynamic heating of the SARA Sub-orbital Platform is simulated, considering the air around the external surface in chemical equilibrium when its temperature reaches 2000 K. The simulation is performed coupling the engineering method for aerodynamic heating with the heat conduction in the wall and ablation of the thermal field. Results show that, although the heat convection parameters are strongly influenced by the chemical equilibrium hypothesis, the resulting wall heat flux is the same when the air is considered a perfect gas.*

Keywords: *Aerodynamic heating, Chemical equilibrium, Computational simulation.*

1. INTRODUCTION

Space and sub orbital vehicles reach high speeds within the atmosphere, i.e., below 100 km of altitude. Such high velocities result in aerodynamic heating. The heat exchange at the wall surface involves heat convection and thermal radiation processes. In the case of recoverable payloads, the heating occurs in both, ascendant and reentry trajectories. Air temperature surpasses 2000^{o} C at the stagnation point (Machado and Pessoa Filho, 2007). As a consequence, aerodynamic heating plays a very important role in the vehicle design. Besides the effects of high temperatures on the mechanical behavior of the structure and onboard devices, it is mandatory to preserve the payload, by using an efficient TPS (Thermal Protection System).

The main source of heat in a hypersonic flight is due the chock front that appears when the velocity surpasses the sound speed in atmospheric flight. The higher is the Mach number, the higher is the air temperature reached after the shock. Such high temperatures are enough to excite the internal vibrational energy of the gaseous molecules, which may cause dissociation and even ionization of them. Thus, the shock layer (flow region forward the shock) can be characterized as a chemically reacting flow. Since those reactions are endothermic, they may reduce the temperature within the shock layer. When the air is considered a perfect gas, without any chemical reaction and with the isentropic constant $\gamma = 1.4$, the temperatures after the shock layer would be quite higher than the actual temperatures.

For air at 1 atm, the following effects appear with the temperature rising (Miranda & Mayal, 2001):

- 800 K: variation of g becomes important;
- 2000 K: Oxygen dissociation begins;
- 4000 K: Oxygen totally dissociated end beginning of Nitrogen dissociation;
- 9000 K: Nitrogen totally dissociated;
- Above 9000 K: Ions formation. The gas becomes partially ionized plasma.

If the chemical reactions and the vibrational excitation develop fast when compared with the time spent for a fluid particle to move in the flow (to cross the distance between the shock and the nose, for example), the flow is considered to be in chemical and vibrational equilibrium. Otherwise, this is considered as a non-equilibrium flow, which is quite difficult to analyze and will not be considered in this work.

The SARA Sub-orbital Platform. Fig.1, is planned as a recoverable platform for experiments in microgravity environment, and is being developed by the Institute of Aeronautics and Space (IAE) of Brazil. It has a total weight of 250 kg and a payload of 25 kg. The orbital version will be able to perform microgravity experiments and keep in an orbit of 300 km during 10 days (Moraes, 1998). SARA trajectory characteristics are showed in Fig. (2)

The objective of this work is to present a computational simulation of the aerodynamic heating and ablative process in the vicinity of the stagnation point during the flight of the SARA Suborbital Platform, taking into account the effects of the two-dimensional conduction and ablation in TPS and considering air in chemical equilibrium during in some critical flight conditions, which will be compared with the perfect gas hypothesis.

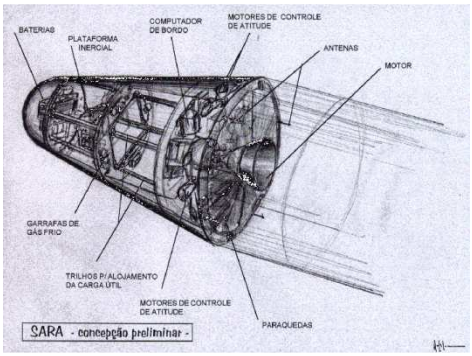

Figure 1. SARA and its subsystems.

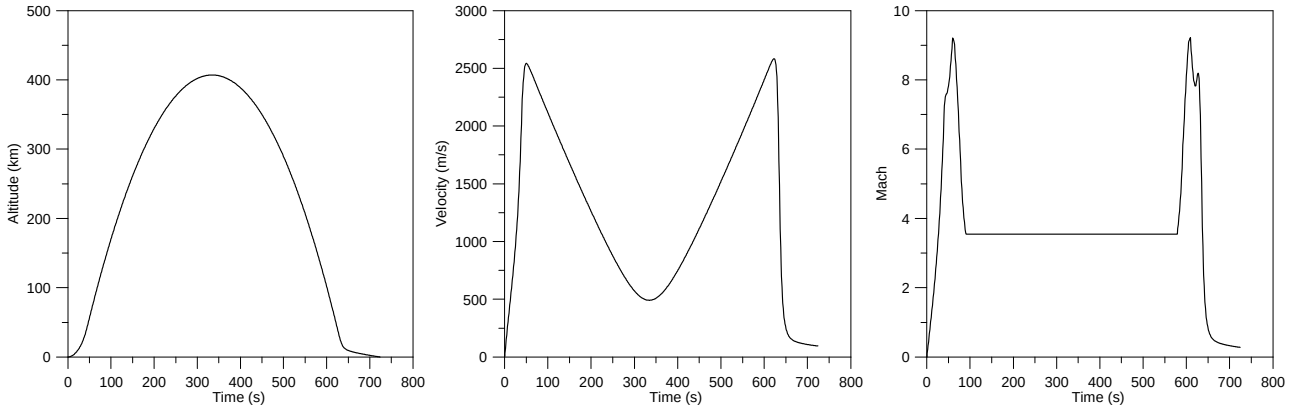

Figure 2. Trajectory of SARA sub-orbital.

2. PHYSICAL PROBLEM AND MATHEMATICAL MODEL

2.1. Aerodynamic heating for perfect gas

To predict the heat transfer on SARA, it is necessary to know pressure, temperature and velocity fields around the vehicle. That can be accomplished by numerically solving the N-S equations. However, such a procedure is expensive and time consuming. In the present work a simpler, but reliable, engineering approach is also used. The following simplifying assumptions are made:

- Zero angle of attack;
- Vehicle rotation around its longitudinal axis is neglected;
- Atmospheric air is considered to behave as a calorically and thermally perfect gas (no chemical reactions)

The free stream conditions ahead of the nose cap are those given by v_∞, T_∞, p_∞, corresponding, respectively, to velocity, temperature and pressure. By knowing v_∞ and altitude, as function of time, together with an atmospheric model (NOAA, 1976), it is possible to evaluate the free stream properties, such as p_∞, T_∞, and c_∞, which represent free stream pressure, temperature and speed of sound, respectively. For supersonic flow ($M_\infty > 1$), a detached shock wave appears ahead of the nose. By using the normal shock relationships (Anderson, 1990), it is possible to calculate v_1, T_1 and p_1 after the shock.

The heat flux over the external surface was calculated through the Zoby's method (Zoby et al, 1981), namely:

$$q = H(T_{aw} - T_w) \tag{1}$$

where q is heat flux, T_w is the wall temperature and T_{aw} is the adiabatic wall temperature, also called recovery temperature, T_r, given by:

$$T_{aw} = T_e + F_R \frac{v_e^2}{2c_p} \tag{2}$$

where c_p is the specific heat, T_e the temperature and v_e the velocity. The subscript e refers to conditions at the boundary layer edge. F_R is the recovery factor, equal to $\sqrt{Pr_w}$, for laminar flow and $\sqrt[3]{Pr_w}$ for turbulent flow. Pr_w is the Prandtl

number evaluated at wall temperature, $Pr_w = 0.71$. The convective heat transfer coefficient comes from the Reynolds analogy, namely:

$$H = 0.5\rho_e c_p v_e \, Pr_w^{-a} \, C_F \tag{3}$$

where a is equal to 0.6 for laminar flow and 0.4 for turbulent flow. To take into account compressibility effects, a modified friction factor is obtained:

$$C_F = K_1 (Re_\theta)^{K_2} \left(\frac{\rho_e^*}{\rho_e} \right) \left(\frac{\mu_e^*}{\mu_e} \right)^{K_3} \tag{4}$$

In the equation above, Re_θ is the Reynolds number, based on the boundary layer thickness, θ:

$$Re_\theta = \frac{\rho_e V_e \theta}{\mu_e} \tag{5}$$

The superscript "*" refers to properties evaluated at Eckert's reference temperature (T_e*). Viscosity, μ, is evaluated according to Sutherland´s equation, as function of temperature and ρ is the specific mass. In Eq.(4) $K_1 = 0.44$, $K_2 = -1$ and $K_3 = 1$, for laminar flow. For turbulent flow, $K_2 = K_3 = -m$, and

$$K_1 = 2 \left(\frac{1}{C_5} \right)^{\frac{2N}{N+1}} \left[\frac{N}{(N+1)(N+2)} \right]^m \tag{6.a}$$

$$m = \frac{2}{N+1} \tag{6.b}$$

$$C_5 = 2.2433 + 0.93N \tag{6.c}$$

$$N = 12.76 - 6.5 \log_{10}(Re_\theta) + 1.21 [\log_{10}(Re_\theta)]^2 \tag{6.a}$$

For laminar flow, the boundary layer thickness is given by (Anderson, 1989):

$$\theta_L = \frac{0.664 \left(\int_0^y \rho_e^* \mu_e^* v_e R^2 dy' \right)^{\frac{1}{2}}}{\rho_e v_e R} \tag{7}$$

where y is measured along the body's surface and $y=0$ corresponds to the stagnation point, and R is a geometric parameter schematically shown in Fig. 3, were the curved red line represents the nose cap surface.

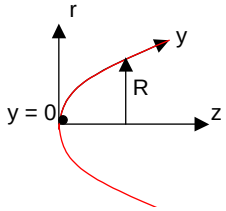

Figure 3. Coordinate system.

In this work the numerical integration of Eq. (7) was obtained according to the trapezoidal method. As $R \rightarrow 0$, Eq. (7) becomes undetermined. By taking the limit of Eq. (7) as $R \rightarrow 0$, the following expression is obtained:

$$\theta_L = \frac{0.332 \left(\rho_e^* \mu_e^* \right)^{\frac{1}{2}}}{\rho_e \sqrt{\frac{1}{R_N} \left[\frac{2(p_s - p_\infty)}{\rho_s} \right]^{\frac{1}{2}}}} \tag{8}$$

In this work Eq. (8) is applied for $y < 0.1 \, R_N$, where R_N is the radius of curvature at the stagnation point.

The boundary layer thickness for turbulent flow is obtained by solving the following first order differential equation:

$$\frac{D\left(\rho_e v_e R\ \theta_T\right)}{Dy} = 0.5 C_F \rho_e v_e R \tag{9}$$

After obtaining the boundary layer momentum thickness, θ, Re_θ, C_F and H can be evaluated by using Eqs. (5), (4) and (3), respectively. Along the transition region between laminar and turbulent flow, the following relationship is used[11]:

$$q_{Tr} = q_L + F(y)(q_T - q_L) \tag{10}$$

where the subscripts *Tr*, *L* and *T* represent, respectively, transitional, laminar and turbulent flow. The transitional factor, *F(y)*, is given by:

$$F(y) = 1 - \exp\left\{-0.412\left[\frac{4.74\left(y - y_L\right)}{\left(y_T - y_L\right)}\right]\right\} \tag{11}$$

Transition is supposed to occur for $163 < Re_\theta < 275$.

Properties evaluation at the boundary layer edge is performed assuming isentropic flow between the stagnation region and the location "*i*" where properties are needed, namely

$$\rho_{e,i} = \rho_s \left(\frac{p_{e,i}}{p_s}\right)^{\frac{1}{\gamma}}\ ;\ h_{e,i} = h_s \left(\frac{p_{e,i}}{p_s}\right)^{\frac{\gamma-1}{\gamma}}\ ;\ v_{e,i} = \sqrt{2\left(h_s - h_{e,i}\right)}\ ;\ T_{e,i} = \frac{h_{e,i}}{c_p} \tag{12}$$

The local pressure, $p_{e,i}$, is obtained from the modified Newton´s method (Anderson, 1989) and $\gamma = 1.4$. The subscript "*s*" appearing in Eqs.(12) refers to the stagnation condition. Eckert's reference temperature is obtained from (Anderson, 1989):

$$\frac{T^*_{e,i}}{T_{e,i}} = 1 + 0.032 M^2_{e,i} + 0.58\left(\frac{T_W}{T_{e,i}} - 1\right) \tag{13}$$

The solution procedure can be summarized as follows:

i. From a given trajectory the US Standard Atmosphere (1976) is used to obtain the free stream properties, including the stagnation ones;
ii. Normal shock relationships are used to obtain the fluid flow properties behind the shock;
iii. By using the modified Newton method, pressure distribution is obtained along the payload;
iv. Equations (12) provide the local properties at the boundary layer edge;
v. If $y < 0.1\ R_N$, Eq. (8) provides the laminar boundary layer thickness, leading to the estimation of Re_θ, C_F and H, provided by Eqs. (5), (4) and (3), respectively;
vi. If $y > 0.1\ R_N$ and $Re_\theta < 163$, Eq. (7) is numerically integrated up to the location where the momentum thickness is to be estimated. Such an integration is performed by using the trapezoidal method;
vii. If $y > 0.1\ R_N$ and $Re_\theta > 275$, Eq. (9) is numerically integrated by the trapezoidal rule leading to the turbulent boundary layer thickness;
viii. If $y > 0.1\ R_N$ and $163 < Re_\theta < 275$, Eqs. (10) and (11) are used to estimate H;

It should be pointed out that such a procedure is performed along the payload's surface (following the *y*-coordinate), for different trajectory times. Therefore, $H = H(y,t)$.

2.3. Aerodynamic heating for chemical equilibrium

The model was extended by Zoby and Moss (1982) for the case of air in chemical equilibrium and its range cover the interval of 1800-8000 km/s and 2-1000 Pa. The model is based in the equations for enthalpy and temperature:

$$\bar{h} = C_h \frac{\bar{P}^m}{\bar{\rho}^n} \tag{14}$$

$$\bar{T} = C_T \frac{\bar{P}^z}{\bar{\rho}^k} \tag{15}$$

Exponents m, n, z and k are equal to 0.97, 0.98. 0,7 and 0,68, respectively. The dimensionless parameters are:

$$\bar{h} = \frac{h}{h_0};\ \bar{T} = \frac{T}{T_0};\ \bar{P} = \frac{P}{P_0};\ \bar{\rho} = \frac{\rho}{\rho_0}\ \bar{\mu} = \frac{\mu}{\mu_0} \tag{16}$$

where reference properties T_0, P_0, ρ_0, and μ_0 are assumed to be 273 K. 1 atm, 1.292 kg/m^3 and 1.715 x 10^{-5} kg/m.s, respectively. For reference enthalpy, $h_0 = RT_0$, where R = 287.1387 J/kg.K.

The constants C_h and C_T are estimated considering a streamline crossing normally the shock front. They are extracted from the following equations:

$$C_h = C_h^* \tag{17}$$

$$C_T = \frac{C_T^*}{e^{CP.BP}} \tag{18}$$

$$C_h^* = \sum_{i=1}^{10} a_i U_h^{i-1} \tag{19}$$

$$C_T^* = \sum_{i=1}^{11} b_i U_T^{i-1} \tag{20}$$

where:

$$CP = \left(\frac{U_T - 20}{18}\right)\left[\left(\frac{U_T - 12}{12}\right)^2\right]^{0.05} \tag{21}$$

$$BP = \frac{\ln\left(\frac{2x10^{-7}}{P\infty}\right)}{50} \tag{22}$$

$$U_h = \left(\frac{2x10^{-5}}{P_\infty}\right)^{\frac{1}{15}}\left(\frac{U_\infty - 2.4384}{2.4384}\right) \tag{23}$$

$$U_T = \frac{U_\infty}{0.3048} \tag{24}$$

In the previous equations, the values for P_∞ and ρ_∞ should be expressed in atm and km/s, respectively. The coeficients of Eqs.(19,20) are given in Tab (1).

The properties aftershock are estimated through the conservation laws:

$$\rho_\infty V_\infty = \rho_A V_A \tag{25}$$

$$P_\infty + \rho_\infty V_\infty^2 = P_A + \rho_A V_A^2 \tag{26}$$

$$h_\infty + \frac{V_\infty^2}{2} = h_A + \frac{V_A^2}{2} \tag{27}$$

From Eqs(25, 26):

$$P_A = P_\infty + \rho_\infty V_\infty^2 - \rho_\infty V_\infty V_A \tag{28}$$

From Eqs.(14, 15):

$$\rho_A = \rho_0 \left[\frac{C_h \overline{P}_A^m}{\overline{h}_A} \right]^{1/n} \tag{29}$$

The sequence to estimate the properties aftershock is:

i. Assume $V_A = 0$;
ii. Obtain P_A from Eq.(28);
iii. Obtain h_A from Eq.(27);
iv. Obtain ρ_A from Eq.(29);
v. Estimate a new value for V_A through Eq.(25);
vi. Repeat steps 2-6 until the desired accuracy is achieved.

After V_A is estimated, obtain T_A from Eq.(15). Stagnation properties are obtained from:

$$h_s = h_\infty + \frac{V_\infty^2}{2} = h_A + \frac{V_A^2}{2} \tag{30}$$

$$\overline{h} = \left\{ \overline{h}_A^{\frac{n-1}{n}} + \frac{1}{C_h^{1/n}} \left(\frac{n-1}{n-m} \right) \left[\overline{P}^{\left(\frac{n-m}{n}\right)} - \overline{P}_A^{\left(\frac{n-m}{n}\right)} \right] \right\}^{\frac{n}{n-1}} \tag{31}$$

$$\overline{P} = \left\{ \overline{P}_A^{\frac{n-m}{n}} + C_h^{1/n} \left(\frac{n-m}{n-1} \right) \left[\overline{h}_s^{\left(\frac{n-1}{n}\right)} - \overline{h}_A^{\left(\frac{n-1}{n}\right)} \right] \right\}^{\frac{n}{n-m}} \tag{32}$$

Since h_s and P_s are known, T_s and ρ_s are estimated through Eqs. (14,15). The Newton Method and Eq. (31) allow to obtain pressure and enthalpy at any point of the body surface. The other properties are calculates through the previous equations for air in chemical equilibrium.

Table 1. Coefficients for Eqs.(19, 20).

i	a_i	b_i
1	4.529228633899	12.297991101529
2	4.446970720900	-8.238094255731
3	1.386555275431	2.419592541157
4	-13.142746144615	-0.33538942364
5	6.997767376225	0.02067595608575
6	21.914473834036	$0.1046732310838 \times 10^{-3}$
7	-34.236435659858	$-0.1014180246941 \times 10^{-3}$
8	20.407510958029	$0.6888281850264 \times 10^{-5}$
9	-5.658335244460	$-0.2245678457584 \times 10^{-6}$
10	0.611030863675	$0.3725350878072 \times 10^{-8}$
11	-	$-0.2518960222376 \times 10^{-10}$

3. RESULTS

The calculation was performed for SARA platform, considering a variable thickness TPS of Quartz-Phenolic resin. The simulation of heat conduction and ablation for the perfect gas hypothesis was previously presented by Machado (2006), were its description can be found. The same method was applied to chemical equilibrium case.

In Fig.(4.a), a remarkable difference between the models for the temperature aftershock can be observed. However, The consequent internal wall temperature resulting of the aerodynamic warming is discreet, Fig.(4.b).

Results show that there are no relevant differences among the results for perfect gas and chemical equilibrium for the heat transfer coefficient, as showed in Fig. (5, left). The heat flux presents similar behavior and the differences are observed only at the peaks during ascendance and reentry, Fig. (5, right).

These results were extended to the rest of SARA's surface. Figure 6 shows the final thickness of TPS along the Y coordinate, tangent to external surface. A small difference is observed near the stagnation point. The perfect gas hypothesis seems to slightly overestimate the TPS mass consumption. However, the difference is not relevant when compared with the total thickness.

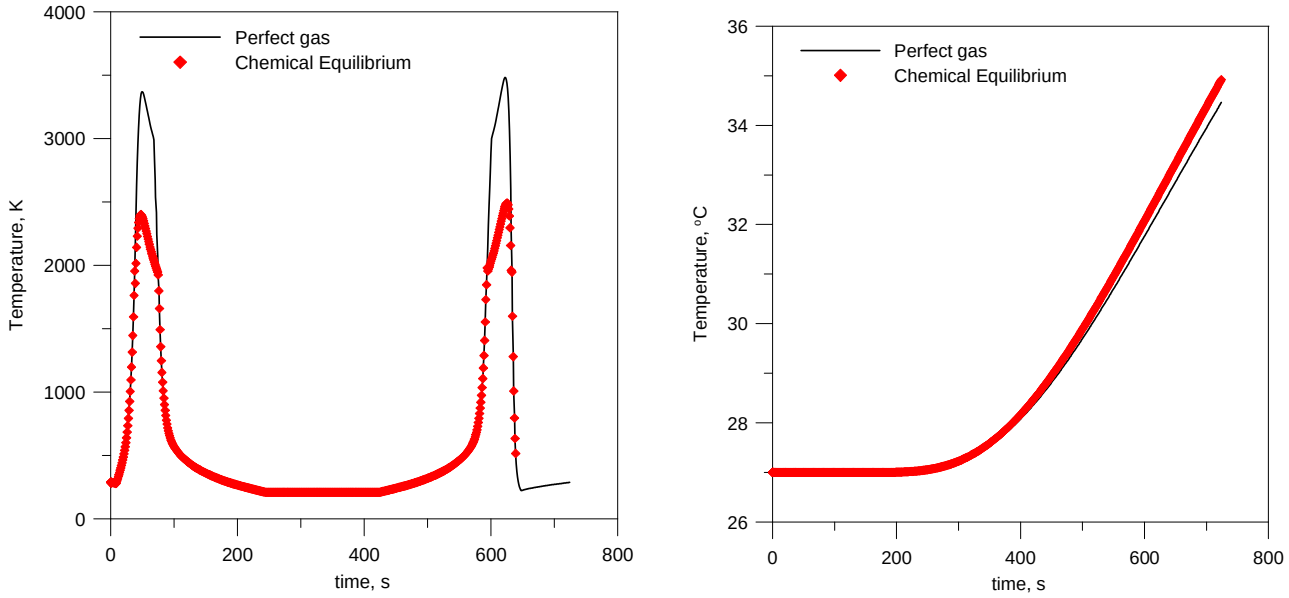

(a) Temperature aftershock *(b) Internal surface*

Figure 4. Temperatures at stagnation point.

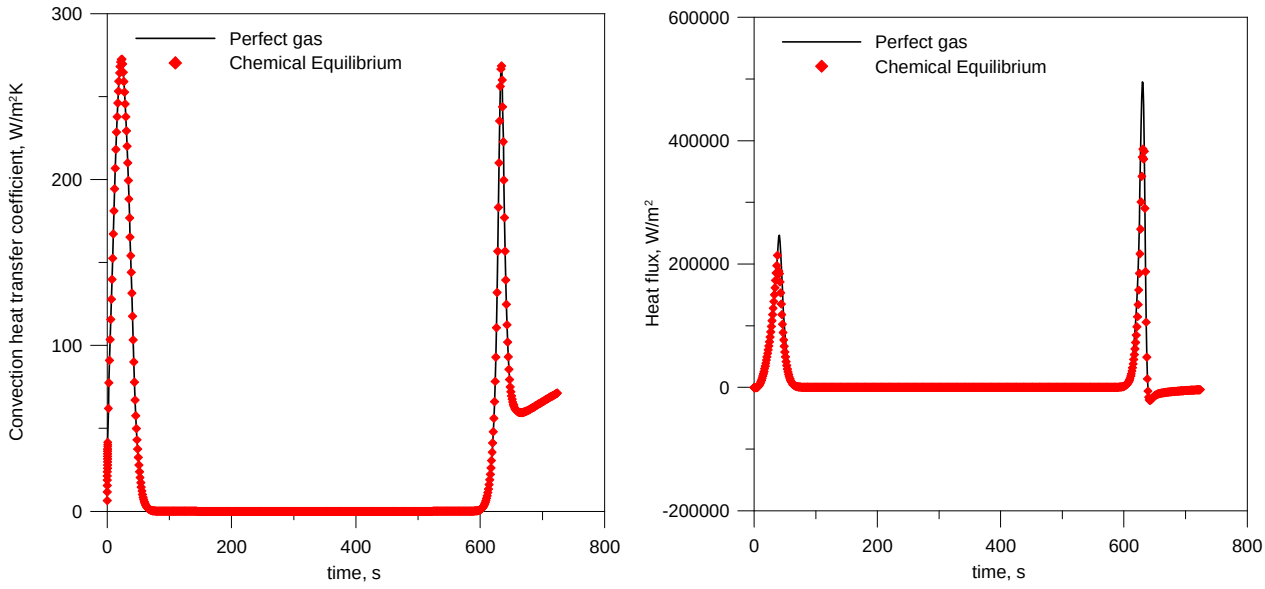

Figure 5. Heat transfer at stagnation point.

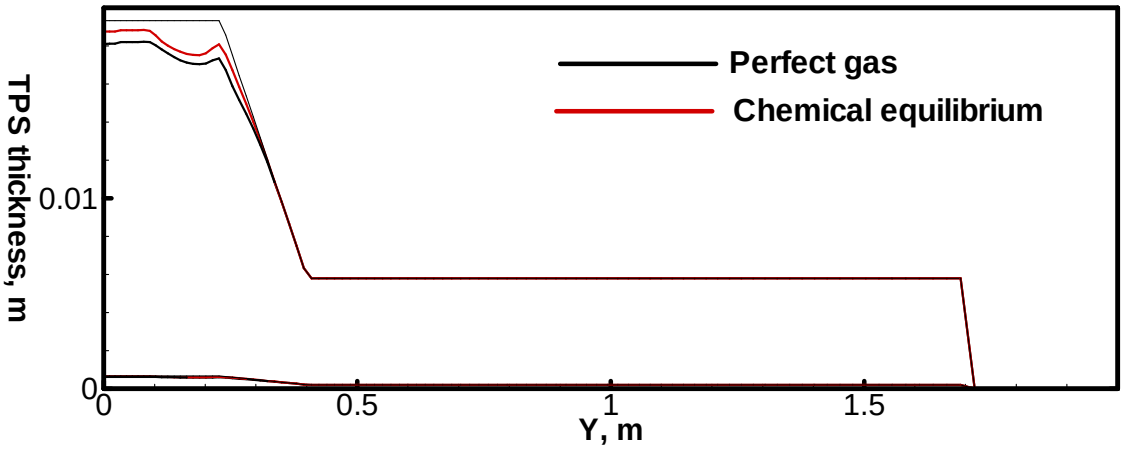

Figure 6. TPS Thickness with y-coordinate at final time.

4. CONCLUSION

The results demonstrated that the hypothesis of chemical equilibrium for air over 2000 K does not present relevant differences when compared with the perfect gas hypothesis for air. However, such approach should be tested for more critical condition, like orbital or planetary reentry.

5. REFERENCES

Anderson Jr., J. D., 1989, "Hyphersonic and High Temperature Gas Dynamics", McGraw-Hill.

Machado, H.A., 2006, "Thermal Protection for Aerodynamic Heating of the Suborbital Sara Capsule", Proceedings of 4th National Congress of Mechanical Engineering, Recife, Brazil. (in Portuguese)

Machado, H.A. and Pessoa-Filho, J.B., 2007, "Aerodynamic Heating at Hypersonic Speeds," Proceedings of 19th Brazilian Congress of Mechanical Engineering, Brasília, Brazil.

Miranda, I.F. and Mayall, M.C de M., 2001, "Convective Heat Flux in Micro-Satellites during the Atmospheric Reentry," Graduate Dissertation, Air Force Technical Institute - ITA, São José dos Campos, Brazil (in Portuguese).

Moraes Jr., P., 1998, "Design Aspects of the Recoverable Orbital Platform SARA", Proceedings of 8th Chilean Congress of Mechanical Engineering, Concepcíon, Chile.

NOAA – National Oceanic and Atmospheric Administration, 1976, U.S. Standard Atmosphere, 1976, U.S. Government Printing Office, Washington, D.C., USA.

Zoby, E.V., Moss, J.N. and Sutton, K., 1981, "Approximate Convective Heat Equations Hypersonic Flows," Journal of Spacecraft and Rockets, Vol. 18, No. 1, pp. 64-70.

Zoby, E.V., Moss, J.N., 1982, "Thermodynamic Equlibrium-Air Correlations for Flowfield Applications," AIAA Journal, Vol. 20, No. 6, pp. 849-854.

6. RESPONSIBILITY NOTICE

The author(s) is (are) the only responsible for the printed material included in this paper.